

The Millennium Galaxy Catalogue: the B -band attenuation of bulge and disc light and the implied cosmic dust and stellar mass densities

Simon P. Driver,^{1*} Cristina C. Popescu,² Richard J. Tuffs,² Jochen Liske,³
Alister W. Graham,⁴ Paul D. Allen¹ and Roberto De Propris⁵

¹*SUPA†, School of Physics and Astronomy, University of St Andrews, North Haugh, St Andrews, Fife, KY16 9SS*

²*Max-Planck-Institut für Kernphysik, Saupfercheckweg 1, 69117 Heidelberg, Germany*

³*European Southern Observatory, Karl-Schwarzschild-Str. 2, 85748 Garching, Germany*

⁴*Centre for Astrophysics and Supercomputing, Swinburne University of Technology, Hawthorn, Victoria 3122, Australia*

⁵*Cerro Tololo Inter-American Observatory, Casilla 603, La Serena, Chile*

Accepted Received

ABSTRACT

Based on our sample of 10095 galaxies with bulge-disc decompositions we derive the *empirical* B_{MGC} -band internal attenuation–inclination relation for galaxy discs and their associated central bulges. Our results agree well with the independently derived dust models of Tuffs et al., leading to a direct constraint on the mean opacity of spiral discs of $\tau_B^f = 3.8 \pm 0.7$ (central face-on B_{MGC} -band opacity). Depending on inclination, the B_{MGC} -band attenuation correction varies from 0.2 – 1.1 mag for discs and from 0.8 – 2.6 mag for bulges. We find that, overall, 37 per cent of all B_{MGC} -band photons produced in discs in the nearby universe are absorbed by dust, a figure that rises to 71 per cent for bulge photons. *The severity of internal dust extinction is such that one must incorporate internal dust corrections in all optical studies of large galaxy samples. This is particularly pertinent for optical HST comparative evolutionary studies as the dust properties will also be evolving.* We use the new results to revise our recent estimates of the spheroid and disc luminosity functions. The implied stellar mass densities at redshift zero are somewhat higher than our earlier estimates: $\rho_{\text{discs}} = (3.8 \pm 0.6) \rightarrow (4.4 \pm 0.6) \times 10^8 h \text{ M}_{\odot} \text{ Mpc}^{-3}$ and $\rho_{\text{bulges}} = (1.6 \pm 0.4) \rightarrow (2.2 \pm 0.4) \times 10^8 h \text{ M}_{\odot} \text{ Mpc}^{-3}$. From our best fitting dust models we derive a redshift zero cosmic dust density of $\rho_{\text{dust}} \approx (5.3 \pm 1.7) \times 10^5 h \text{ M}_{\odot} \text{ Mpc}^{-3}$. This implies that $(0.0083 \pm 0.0027) h$ per cent of the baryons in the Universe are in the form of dust and $(11.9 \pm 1.7) h$ per cent (Salpeter-‘lite’ IMF) are in the form of stars (~ 58 per cent reside in galaxy discs, ~ 10 per cent in red elliptical galaxies, ~ 29 per cent in classical galaxy bulges and the remainder in low luminosity blue spheroid systems/components).

Key words: galaxies: spiral – galaxies: structure – galaxies: photometry – galaxies: fundamental parameters – ISM: dust, extinction

1 INTRODUCTION

Internal dust attenuation of the photon flux from galaxies is a severe issue at optical wavelengths, reducing the total emergent luminosity, introducing an inclination dependence of the observed flux (e.g., Giovanelli et al. 1995; Masters et al. 2003) and modifying the galaxy light-profile shape. Model predictions of these effects have been given by many authors, including Kylafis & Bahcall 1987; Byun, Freeman & Kylafis 1994; Evans 1994; Kuchinski et al. 1998; Bianchi et al. 1996; Ferrara et al. 1999; Baes & Dejonghe 2001; Cunow 2001; Tuffs et al. 2004; Pierini et al. 2004; Möllenhoff et al. 2006). Typically, spiral galaxies exhibit a radial

gradient in opacity, with higher opacities in the central regions (Boissier et al. 2004; Popescu et al. 2005). The dust is also typically distributed in a thinner layer than the stellar population(s) (Xilouris et al. 1999). Because of these two properties of the dust distribution, the *observed* stellar profiles appear less centrally concentrated (i.e., lower Sérsic indices), scale-lengths are overestimated, luminosities are underestimated and the central surface brightnesses artificially dimmed. All of these effects become more pronounced at higher inclinations¹ (see Möllenhoff et al. 2006 for detailed model predictions). Dust may also exacerbate the issue of inner disc trun-

* E-mail: spd3@st-and.ac.uk

† Scottish Universities Physics Alliance

¹ Here we define inclination to run from face-on (low inclination, $i = 0$ deg) to edge-on (high inclination, $i = 90$ deg).

cation leading to Type II profiles (Freeman 1970) by preferentially suppressing core flux.

Bulges, even though they are assumed to contain minimal dust, are still seen through the dust layer of the disc, and therefore also suffer attenuation of their stellar light and modification of their surface-brightness distributions due to dust. In fact, these effects are predicted to be even more pronounced for bulges than for the discs (Tuffs et al. 2004), since bulges are concentrated towards the central regions of galaxies, where the opacity is highest.

In terms of obtaining statistical distributions for the disc and bulge components (e.g., disc/bulge luminosity–size or luminosity–colour distributions, see Driver et al. 2006), samples uncorrected for galaxy inclination will have their intrinsic distributions broadened (and skewed, see in particular the recent papers by Choi, Park & Vogeley 2007; and Shao et al. 2007). Indeed, recent observational studies have produced evidence that the size distribution of galaxies, at fixed luminosity, is broader than that predicted from hierarchical simulations (see Shen et al. 2003; Driver et al. 2005). In terms of the total stellar mass the effect is less obvious. This quantity is usually estimated by multiplying a galaxy’s luminosity by its stellar mass-to-light ratio, which is in turn derived from the correlation between mass-to-light ratio and colour (Bell & de Jong 2001). The point is that the decrease in the estimated stellar mass due to attenuation will be counteracted, at least to some extent, by the increase in the stellar mass due to reddening. Bell & de Jong (2001) argue that these two effects mostly cancel (see their fig. 1). We find that while this is true for moderately inclined systems ($i < 60$ deg) it does not hold for highly inclined systems.

Historically, there has been some debate as to whether studies of galaxies at various inclinations can be used to constrain the dust distribution and opacity simultaneously (Holmberg 1958; Disney et al. 1989; Valentijn 1990; Disney et al. 1992). The general consensus was that one could not (see Davies & Burstein 1995) and alternative paths to the dust distributions have now been pursued (e.g., overlapping galaxies, Keel & White 2001; surface brightness–scale-length relations, Graham 2001; quasar sight-lines through foreground galaxies, Östman, Goobar & Mortzell 2006; and self-consistent modelling of the UV/optical/FIR/sub-mm emission from galaxies, Silva et al. 1998; Bianchi et al. 2000; Popescu et al. 2000; Popescu & Tuffs 2004). However, with the dust models (including 3D distribution, clumpiness and grain composition) now constrained by independent methods, it should be possible to revisit the use of large statistical catalogues to constrain the mean opacity of discs.

In particular, given a complete galaxy sample with comprehensive structural analysis and high-completeness redshift coverage one should be able to determine, *empirically*, the attenuation–inclination relation.² This can be achieved if a characteristic feature can be identified in the galaxy population and this feature measured for sub-samples of varying inclination. One obvious feature is the turn-over of the luminosity function, i.e. L^* or M^* , which in the absence of dust should be inclination independent. Using large galaxy samples drawn from contemporary surveys M^* can now be measured to an accuracy of $\Delta M^* < 0.1$ mag (see for example Zucca et al. 1997; Norberg et al. 2001; Blanton et al. 2003; Driver et al. 2005).

Predictions based on detailed dust models suggest that the to-

tal B -band magnitude of a galaxy disc may be attenuated by up to 2 mag and that of a galaxy bulge by up to 2.5 mag, depending on opacity and viewing angle (see Tuffs et al. 2004; Pierini et al. 2004). In this paper we report our empirical estimate of the relationship between attenuation and inclination, and use it to constrain the mean opacity of discs by comparison to the model predictions of Tuffs et al. (2004; which in turn are based on the dust model of Popescu et al. 2000). Using a combination of (i) our empirical correction to remove the inclination dependent attenuation, and (ii) the dust model to evaluate and remove the face-on attenuation, we revise the luminosity functions and total stellar mass densities recently reported in Driver et al. (2007). We also combine the mean opacity of discs and total disc stellar mass to derive the cosmic dust density.

In Section 2 we review the data used in this investigation and in Section 3 we describe our empirical analysis leading to a constraint on the mean opacity of galaxies. In Section 4 we use our results to constrain our adopted dust model (Tuffs et al. 2004). In Section 5 we recover the spheroid and disc luminosity functions through a variety of methods and discuss the implications of our findings in the context of the cosmic baryon budget. Throughout we adopt the following cosmological parameters: $\Omega_M = 0.3$, $\Omega_\Lambda = 0.7$ and $H_0 = 100 h \text{ km s}^{-1} \text{ Mpc}^{-1}$.

2 THE MILLENNIUM GALAXY CATALOGUE

The Millennium Galaxy Catalogue (MGC) spans a 37.5 deg^2 region of the vernal equatorial sky and contains 10095 galaxies brighter than $B_{\text{MGC}} = 20$ mag with 96 per cent spectroscopic redshift completeness. The imaging catalogue is described in Liske et al. (2003), the spectroscopic follow-up in Driver et al. (2005) and the photometric accuracy and completeness in Cross et al. (2004), Driver et al. (2005) and Liske et al. (2006). We have decomposed this sample into bulges and discs with GIM2D (Simard et al. 2002), using an $R^{1/n}$ Sérsic profile for bulges and an exponential profile for discs (Allen et al. 2006) and providing an extensive bulge-disc resource which is publicly available at <http://www.eso.org/~jlliske/mgc/>. In this paper we use the MGC structural catalogue MGC_GIM2D.

We point out that not all galaxies in our catalogue are two-component systems. Allen et al. (2006) divided those objects that were best fit with a single-component Sérsic profile into pure discs and pure bulges (i.e. ellipticals) according to their Sérsic index. Note that we use the term ‘spheroid’ to mean both ellipticals and bulges, and we reserve the term ‘bulge’ exclusively for the central 3D structure of a two-component system. We further separate our ellipticals into classical (red) and new (blue), as well as our bulges into classical and pseudo at $(u - r)_{\text{core}} = 2$ mag according to the spheroidal colour bimodality found by Driver et al. (2007, see their fig. 2). In Sections 3 and 4 we will use the classical bulges, but not the ellipticals which are assumed dust free, as well as all of the discs, irrespective of whether they ‘contain’ a bulge or not.

The robustness of our catalogue has been quantified using independent repeat observations and GIM2D decompositions of 682 galaxies. These duplicate observations originate from the overlap regions of neighbouring MGC fields and hence they include the effects of varying observing conditions. This comparison sample demonstrates that for components with $M_B < -17$ mag our structural catalogue is accurate to better than ± 0.1 mag for bulges and ± 0.15 mag for discs, and that the disc inclination, i , has $\Delta \cos(i) \sim 0.05$ (see fig. 15 of Allen et al. 2006). In our analy-

² We note that attenuation is an integral property of an extended distribution of light and should not be confused with the extinction along a single line of sight.

sis we use bin sizes of 0.1 for $\cos(i)$ and 0.5 mag for luminosity. Hence the errors are smaller than the bin sizes in use and much smaller than the size of the expected signal on the magnitudes due to dust (see Möllenhoff et al. 2006).

3 ANALYSIS

The MGC structural parameters we require are the GIM2D total luminosity, the bulge-to-total flux ratio (B/T), the redshift, the redshift quality, the disc inclination and the bulge and disc colours. Of these parameters only the disc inclination requires some adjustment as these were derived under the assumption that galaxy discs are infinitely thin (i.e., $\cos(i) = b/a$, where a and b are the major and minor axes, respectively). In reality discs exhibit a finite thickness preventing b from reaching a value of zero. To accommodate disc thickness we adjust our inclinations according to Hubble (1926): $\cos^2(i) = [\cos^2(i_{\text{GIM2D}}) - Q^2]/(1 - Q^2)$, where Q is the ratio between the disc scale-height and the major axis, and is set here to 0.074 (Xilouris et al. 1999).

In the following we will often use the term ‘inclination’ in connection with bulges. The ‘bulge inclination’ is simply the inclination of the associated disc.

To derive the internal attenuation–inclination relation [i.e., ΔM^* vs. $1 - \cos(i)$] we iteratively follow the procedure outlined below for both bulges and discs. Iteration is required because any B/T and magnitude cuts should be based on the intrinsic values rather than the apparent values:

(i) Extract all discs and bulges and apply the current best estimates of the disc and bulge attenuation–inclination corrections (no correction is applied for the first iteration).

(ii) Recompute all B/T luminosity ratios.

(iii) Select components with $B_{\text{MGC}} < 20$ mag and whose parent galaxies have $B/T < 0.8$.³

(iv) Derive the luminosity distribution (LD) using step-wise maximum likelihood (SWML) for all discs and bulges with low inclination [$1 - \cos(i) < 0.3$].

(v) Fit Schechter functions to the LDs (using only data down to $M_B < -17$ mag) in order to obtain the global value of the faint-end slope, α , for discs and bulges of low inclination.

(vi) Derive the disc and bulge LDs for the full sample in uniform $\cos(i)$ intervals.

(vii) Fit Schechter functions ($M_B < -17$ mag) with α fixed to the global value from step (v).

(viii) Plot the recovered M^* (turn-over luminosity) versus $1 - \cos(i)$.

(ix) Determine the new inclination corrections by fitting equation (1) below to the bulge and disc data using the Levenberg-Marquardt χ^2 minimisation method.⁴

(x) Repeat the above until convergence.

In deriving the LDs using SWML we follow Driver et al. (2007) (for full details of the SWML method consult Efstathiou,

Ellis & Peterson 1988). Briefly, we assume that discs evolve according to $L_z \propto (1 + z)^{-1}$ and we use the globally derived k-corrections for the disc components throughout. For the bulges we adopt a milder evolution of $L_z \propto (1 + z)^{-0.5}$ and use a fixed red bulge k-correction of $k(z) = 3.86z + 12.13z^2 - 50.14z^3$ which is the best fit to an Sa 15.0 Gyr spectrum (see Poggianti 1998). For further details and justification of these choices see Driver et al. (2007).

Crucial to a correct implementation of SWML is the specification of the appropriate flux limit to which each galaxy could have been observed. The flux limit of the MGC spectroscopic survey was $B_{\text{MGC}} = 20$ mag, in Galactic-extinction-corrected Kron magnitudes, and normally this would be the appropriate limit. However, we have since revised our photometry by replacing Kron with profile-extrapolated GIM2D magnitudes. The difference between these is generally small (see fig. 4 of Allen et al. 2006) but it necessitates the introduction of an individual magnitude limit for each galaxy. More significant is that in implementing our dust attenuation correction these magnitude limits must be further adjusted (in effect the correction is analogous to a revision of the photometry). Hence the appropriate magnitude limit to which each galaxy could have been observed is given by: $B_{\text{lim}} = 20 + M_B^{\text{T}}(\text{GIM2D}) - M_B^{\text{T}}(\text{Kron}) + M_B^{\text{C}}(\text{dust corrected}) - M_B^{\text{C}}$, where the superscripts T and C refer to ‘total’ and ‘component’, respectively, and 20 mag is the sample’s original limit in total-galaxy, dust-uncorrected Kron magnitudes. Due to the bulge-disc decomposition it is possible, in fact frequently the case, that a galaxy component may lie below its parent galaxy’s flux limit. In these cases the component is rejected. Keeping these components, i.e. applying the flux limits only to the galaxies, but not their components, would introduce a bias: for example, a bulge with some apparent magnitude below its parent galaxy’s limit would still be included in the sample if it were from a low- B/T system but not if it were from a high- B/T system. Applying the flux limits to the components significantly reduces the sample size but ensures that it remains unbiased. A by-product is that all remaining components will be of high signal-to-noise.

For step (ix) above we arbitrarily choose a power-law to parameterise the attenuation–inclination relation:

$$M_i^* - M_0^* = k_1 [1 - \cos(i)]^{k_2}, \quad (1)$$

where M_i^* refers to the turn-over magnitude at inclination i and M_0^* refers to the face-on turn-over magnitude.

Fig. 1 shows the initial and final iterations for bulges (panels a and b) and discs (panels d and e), where the components have been drawn from galaxies with $B/T < 0.8$ and have $M_B < -17$ mag. From Fig. 1 we can see that both bulge and disc magnitudes are severely underestimated in edge-on systems and a significant correction is required. The final results (after 14 iterations) for the attenuation–inclination relations are:

$$(M_i^* - M_0^*)_{\text{disc}} = (0.99 \pm 0.02) [1 - \cos(i)]^{(2.32 \pm 0.05)} \quad (2)$$

and

$$(M_i^* - M_0^*)_{\text{bulge}} = (2.16 \pm 0.1) [1 - \cos(i)]^{(2.48 \pm 0.12)}. \quad (3)$$

These relations are shown as solid lines in the central panels of Fig. 1. We also show the initial relations (before any iteration) as dotted lines. We can see that the iteration process actually has a fairly small effect on both the disc and bulge solutions. Fig. 2 shows the convergence path for the disc and bulge solutions. The discs converge almost instantly whereas the bulge solution shows more variation. This in part reflects the larger disc sample but may also indicate more noise in the bulge data as one might expect for the

³ The fixed cut at $B/T < 0.8$ is necessary as the post-GIM2D processing of our catalogue (see Allen et al. 2006, fig. 14) replaces all systems with higher B/T values with single Sérsic-only fits (as is common practice in detailed surface photometry), thereby re-defining them as ellipticals.

⁴ During the fitting process the highest inclination bin is ignored as the accuracy of the bulge-disc decomposition is susceptible to break-down at this limit and, as we shall see later, this bin remains incomplete.

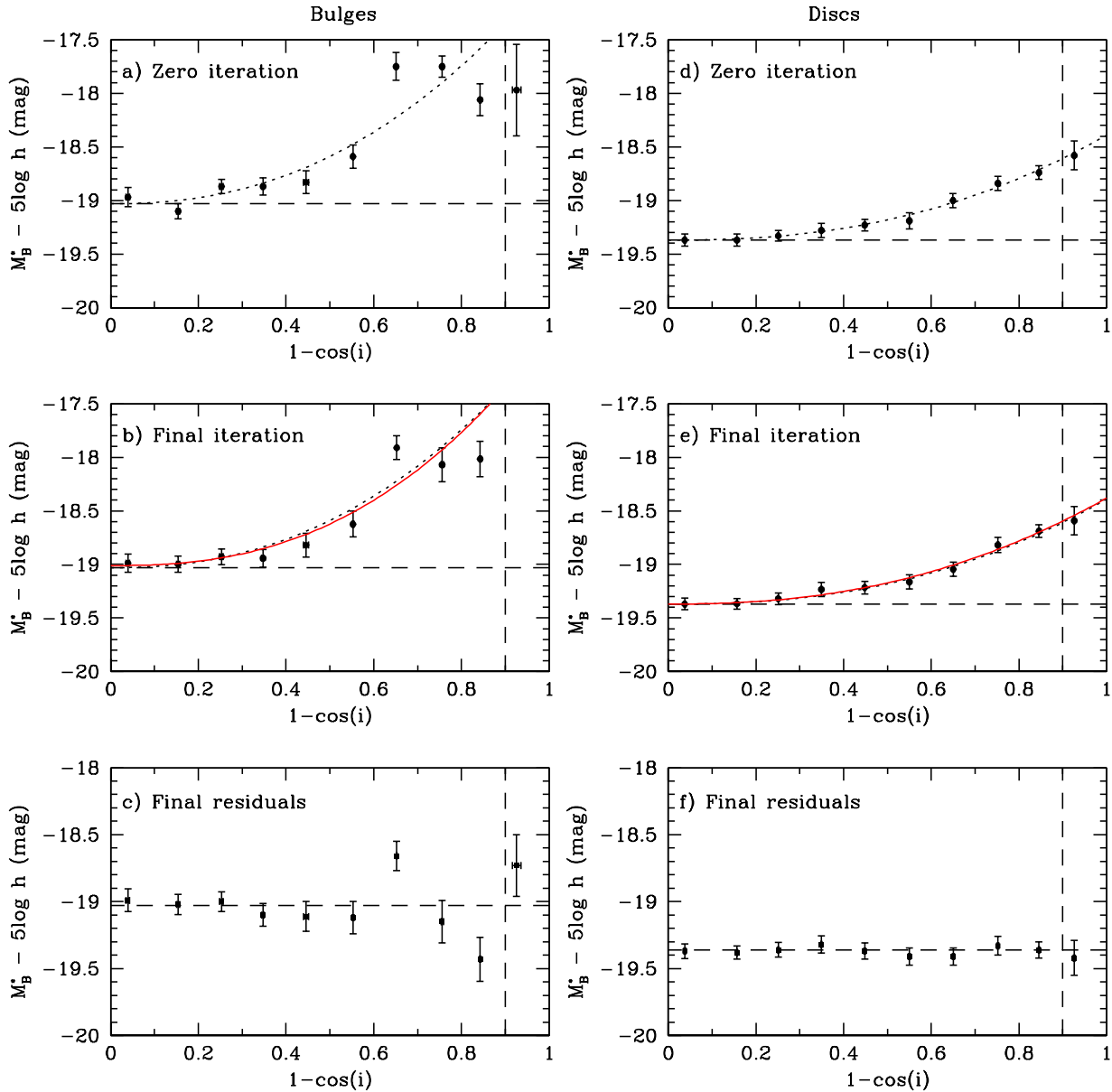


Figure 1. Panels (a) and (d) show the derived M_B^* values for bulges and discs as a function of $1 - \cos(i)$ based on the raw data. All components are drawn from galaxies with $B/T < 0.8$ and have luminosities $M_B < -17$ mag. The dotted line shows the best fit of equation (1) to these data, using only the points at $1 - \cos(i) < 0.9$ (marked by the vertical dashed line). Panels (b) and (e) show the final results after applying the inclination corrections and re-deriving the attenuation-inclination relations repeatedly until stable solutions are reached. The solid lines show the final fits to these data, while the dashed lines are the same as in panels (a) and (d). The disc relation is barely changed by the iteration and the bulge relation has evolved only mildly. The lower panels (c and f) show the residuals between the data points and the solid line fits.

less well resolved component. As the solutions are dependent on each other it is reassuring that the disc solution is robust to the variations in the bulge solution.

3.1 Robustness checks

As our result is fairly striking and the implications potentially far-reaching, it is important to ensure our interpretation is correct and

not due to some systematic artifact of the bulge-disc decomposition process. Below we outline a number of checks which we use to reassure ourselves, and the reader, that the result is robust and accurately described by the equations shown above.

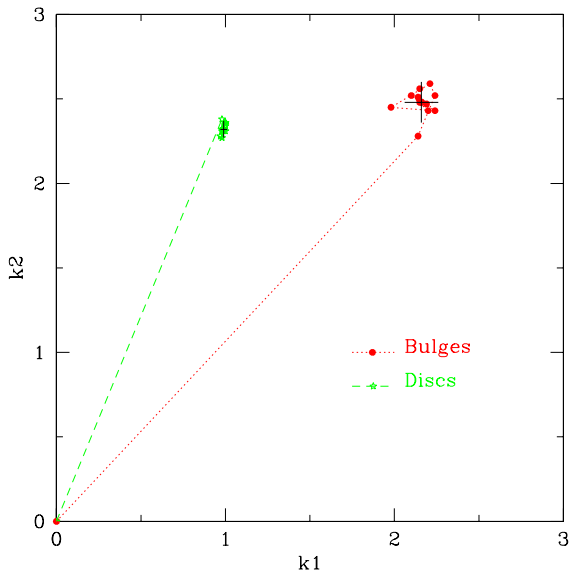


Figure 2. The paths of convergence for the iterative fitting of equation (1) to the disc and bulge data as indicated. It is clear that the disc solution is extremely stable with the bulge solution drawing out a larger error distribution in the two fitted parameters. The solid crosses mark the final solutions and associated errors.

3.1.1 The luminosity function fits

Figs. 3 and 4 show the individual luminosity functions for discs and bulges for each $1 - \cos(i)$ interval before (dotted lines) and after (solid lines) implementing the dust-induced inclination correction. To provide a reference we show as long dashed lines the luminosity functions derived from bulge or disc components with $1 - \cos(i) < 0.3$, scaled down by a factor of 3 to account for the 3 times larger range in $1 - \cos(i)$. In general the luminosity distributions are well behaved and the Schechter function fits are all good. The uncorrected data (open circles) show a significant and progressive shift to fainter M^* values at higher inclinations. The corrected data (filled circles) show that the M^* values are now consistent, as required by the fitting process. However, we can also see that the normalisations are also consistent (cf. dashed comparison line) both for the bulge and disc populations. The only significant inconsistency is in the final, highest inclination bin where the normalisations are low, suggesting some residual incompleteness. As the highest inclination bin was not used in the fitting process this does not affect our attenuation–inclination solutions.

3.1.2 The $1 - \cos(i)$ distribution

The upper panels of Fig. 5 show the $1 - \cos(i)$ distributions before and after implementing the attenuation–inclination corrections. For a randomly orientated sample of thin discs the $1 - \cos(i)$ distributions should be constant. Note that the magnitude limits used in these plots are dictated by the nominal limit of the MGC survey ($B_{\text{MGC}} = 20$ mag) minus the maximum bulge and disc corrections (i.e., ~ 1.5 and 1.0 mag, giving limits of 18.5 and 19.0 mag respectively). Fainter than these limits our samples become incomplete, with the incompleteness depending on inclination.

From Fig. 5 we can see that the raw data (dotted lines) show a strongly skewed distribution implying significant incompleteness towards the high-inclination end, providing corroborating evidence

of the severe effect of dust attenuation. Furthermore, bulges show a more extreme skew than discs implying that a larger correction is required for the bulges as shown by equations (2) and (3). After implementing the corrections described above, both distributions are now flat. We consider both the flatness of the $1 - \cos(i)$ distribution and the uniformity of the normalisations of the Schechter function fits from Figs. 3 and 4 to be extremely strong independent evidence that our derived corrections are caused by dust attenuation and that equations (2) and (3) are correctly accounting for this effect. Note that the $1 - \cos(i)$ distributions also show some residual incompleteness in the highest inclination bin, potentially requiring the final space density of bulges and discs to be increased by factors of 1.05 and 1.06, respectively.

3.1.3 Solutions for restricted B/T ranges

An obvious concern is that the empirical correction may depend on the bulge-to-total flux ratio, B/T . Fig. 6 shows the trends for three different B/T ranges as defined by the horizontal bands shown in the lower panels of Fig. 5. To construct these plots we initially adopted the solutions derived from the full sample and then followed the iterative procedure outlined in Section 3. The data for low B/T bulges (Fig. 6a) is particularly sparse (see also lower left panel of Fig. 5) and therefore not particularly informative, while the worst statistics for discs are found in the high B/T sample (panel f). Hence we will only compare the results from the intermediate and high B/T bulge sub-samples (panels b and c) and from the low and intermediate B/T disc sub-samples (panels d and e).

The disc correction seems reasonably insensitive to B/T . For bulges there may be a tendency towards a shallower attenuation–inclination relation for higher B/T systems. Three potential explanations for such a trend immediately come to mind: (i) an intrinsic variation in the opacity of discs with B/T ; (ii) a variation in the size of bulges relative to the scale-length of the dust disc (such that the effective radius of the bulge becomes comparable to the scale-length of the dust in high B/T systems); and (iii) a systematic error in our bulge-disc decompositions such that flux is transferred from bulges to discs preferentially for lower B/T systems.

The uniformity of the disc relation argues against (i). One might also expect it to rule out (iii). However, although the transfer of flux from bulges to discs in low B/T systems can significantly modify the flux of the bulge, it will actually have a much smaller impact on the disc fluxes (because the systems have low B/T). In Section 4 we will show that the dust model prediction for the low B/T disc sample actually reproduces the bulge trend for the high B/T sample reasonably well. This suggests that (ii) is unlikely to be the correct explanation. We therefore conclude that we may be slightly underestimating the flux of the bulges of low B/T systems due to the bulge-disc decomposition, preferentially re-assigning flux from the bulge to the disc at higher inclinations, although we cannot rule out a real phenomenon, not predicted by models.

Arguably, the above implies that it may be better to construct bulge luminosity functions from face-on samples as opposed to implementing the inclination correction. The disc sample on the other hand is robust with respect to variations in B/T , indicating that dust properties scale with the disc, as one would expect, and are entirely independent of the bulge.⁵ For the discs our correction is

⁵ Note that we have already applied a colour cut to our bulge sample to remove contaminating blue pseudo-bulges.

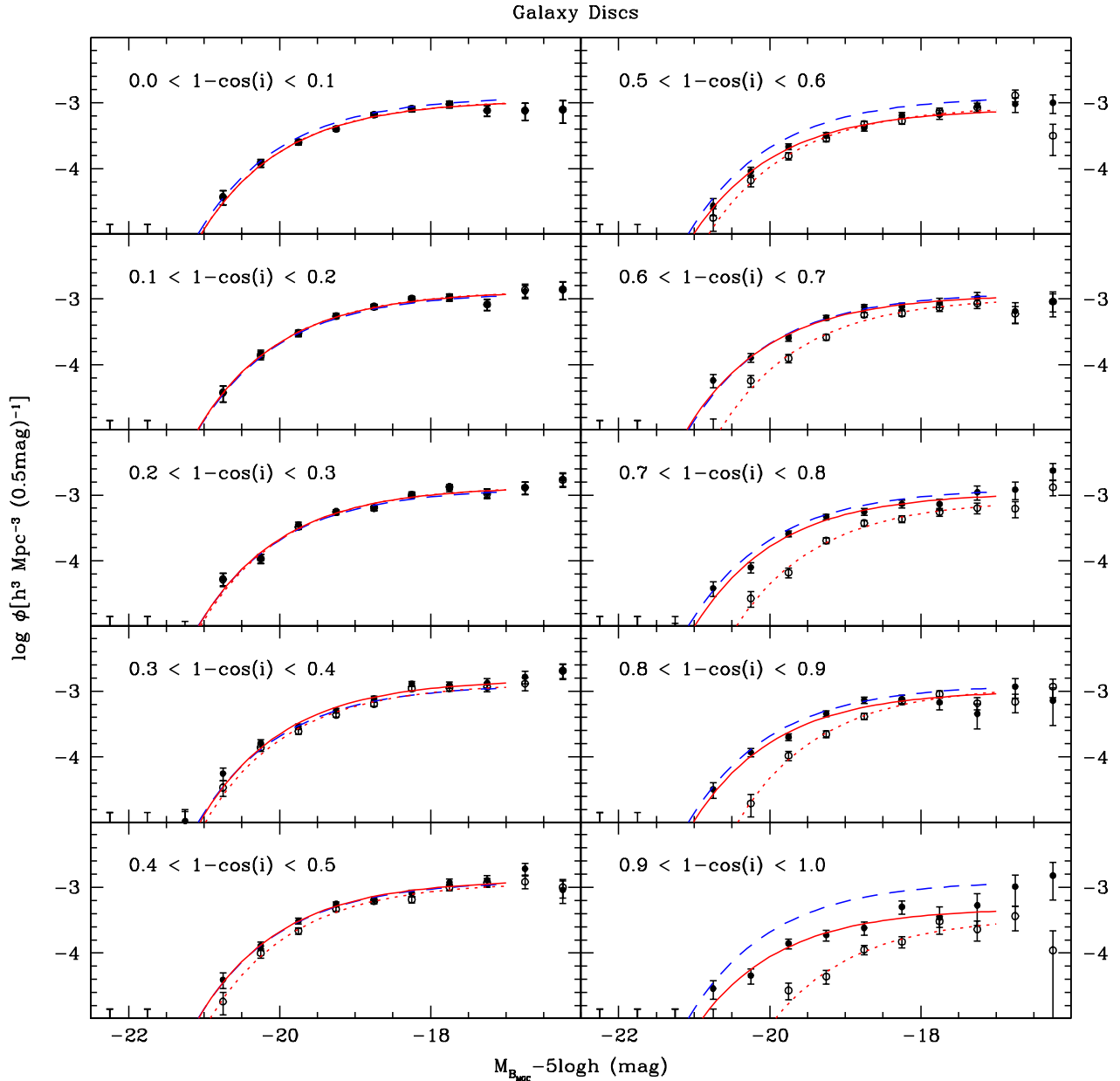


Figure 3. Each panel shows the disc luminosity distribution for an inclination-selected sub-sample (as indicated) before (open circles) and after (filled circles) attenuation–inclination correction. The red solid and dotted lines show Schechter function fits to the corrected and uncorrected data, respectively. For reference, we also show as a blue dashed line the Schechter function derived from all discs with $1 - \cos(i) < 0.3$, scaled down by a factor of 3.

therefore applicable over the full B/T range. Hence we will continue to use the bulge correction based on the full sample.

3.1.4 Comparison of attenuation-corrected LFs and uncorrected face-on LFs

A further check is to re-derive the bulge and disc luminosity distributions without applying the inclination dependent dust correction but using face-on systems only. These should agree with the full-sample, corrected distributions provided the normalisations are

adjusted appropriately (although the errors of the scaled-up face-on sample are expected to be higher). Fig. 7 shows the results which are also tabulated in Table 1. Rows 4 and 5 show the results for the disc luminosity functions derived from data restricted to $1 - \cos(i) < 0.3$ and scaled up by a factor of 3.33. These face-on estimates essentially circumvent the entire empirical attenuation–inclination fitting process. The two luminosity function estimates

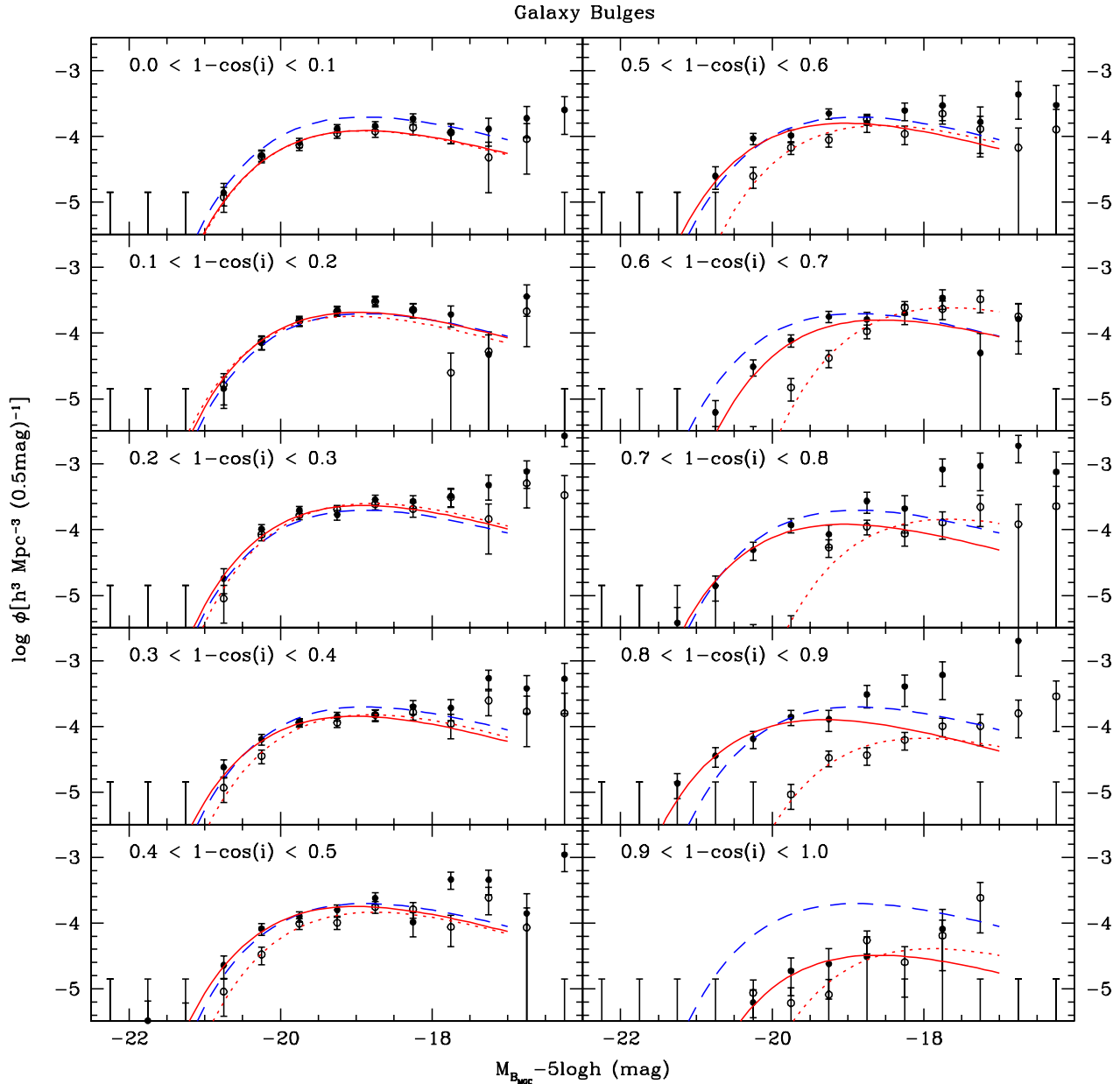


Figure 4. Each panel shows the bulge luminosity distribution for an inclination-selected sub-sample (as indicated) before (open circles) and after (filled circles) attenuation–inclination correction. The red solid and dotted lines show Schechter function fits to the corrected and uncorrected data, respectively. For reference, we also show as a blue dashed line the Schechter function derived from all bulges with $1 - \cos(i) < 0.3$, scaled down by a factor of 3.

agree well with just a slight offset in normalisation.⁶ Based on the 1σ error contours (right panels in Fig. 7) the face-on data agree with the inclination corrected data and both are formally inconsistent with the results from the full, uncorrected sample. Note that the error contour for the face-on sample is larger than the others as the sample is of course smaller.

⁶ The inclination corrected luminosity functions have been scaled slightly to account for the residual incompleteness factors derived in Section 3.1.2.

3.1.5 GIM2D Robustness

The general robustness of GIM2D has been extensively verified via a number of studies, in particular Simard et al. (2002), who use detailed simulations to verify the accuracy of the code. Comparisons have also been made against other similar codes (e.g., Pignatelli, Fasano & Cassata 2006). Generally GIM2D has no systematic bias, except perhaps with the recovery of large Sérsic indices ($n > 4$). Overall it is generally considered a robust and reliable code. Here we do not repeat these studies however we do address the credibility of our measurements via repeat analyses for a subset of galaxies

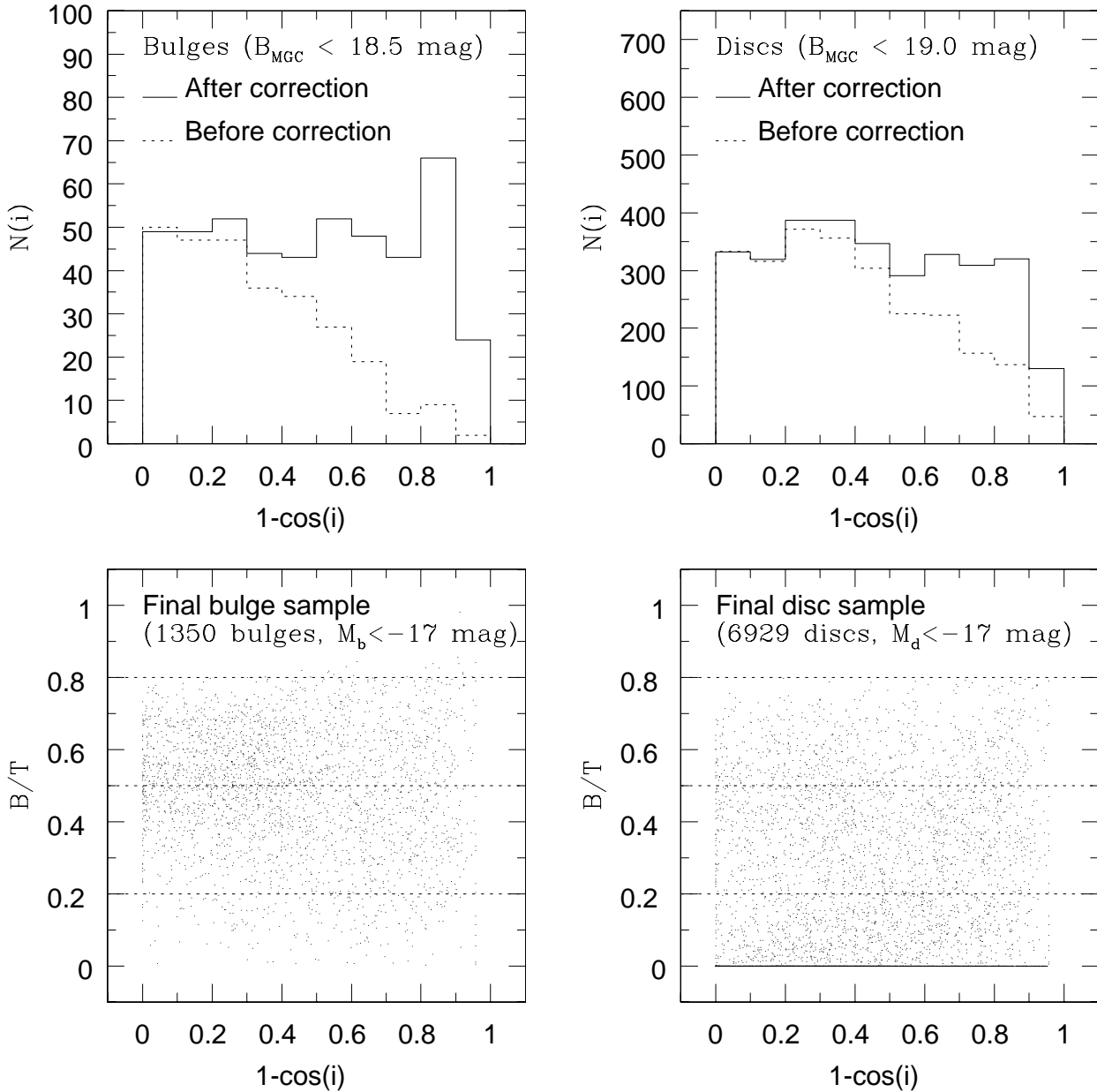


Figure 5. The upper panels show the $1 - \cos(i)$ distributions of bulges (left) and discs (right) before (dotted lines) and after (solid lines) applying the inclination dependent magnitude correction. In the lower panels we plot B/T versus $1 - \cos(i)$ for the corrected data.

which lie in the overlap regions (see Liske et al. 2003). From the overlap regions we have 682 repeat observations for which identical bulge disk decompositions analyses and logical filtering (see Allen et al. 2006) have been carried out. In this paper we are only using high signal-to-noise components where the component magnitude is brighter than 20.0 mag, the absolute component magnitude is brighter than -17.0 mag, and where the apparent- B/T ratio is less than 0.5. After implementing these cuts in both set of analyses we are left with a total of 20 bulges and 389 discs for which repeat GIM2D measurements exist. Fig. 8 shows the stability of the key measurements ($1 - \cos(i)$ and component magnitude) — note that

the inclination adopted for the bulge components is taken from their associated discs. These data confirm the broader analysis of the full catalogue by Allen et al. (2006) that our GIM2D measurements are repeatable. The component magnitudes are robust to better than ± 0.1 mag (for both bulges and discs) and that the $1 - \cos(i)$ measurement is robust to ~ 0.05 for systems with high signal-to-noise bulges and ~ 0.1 for disc systems. As the error in $1 - \cos(i)$ is comparable to our bin size, for discs, this may partially explain the smooth trend where scattering between bins will correlate both the measurements and errors. It is worth noting that the accuracy of the disc inclination appears more robust for those systems with a

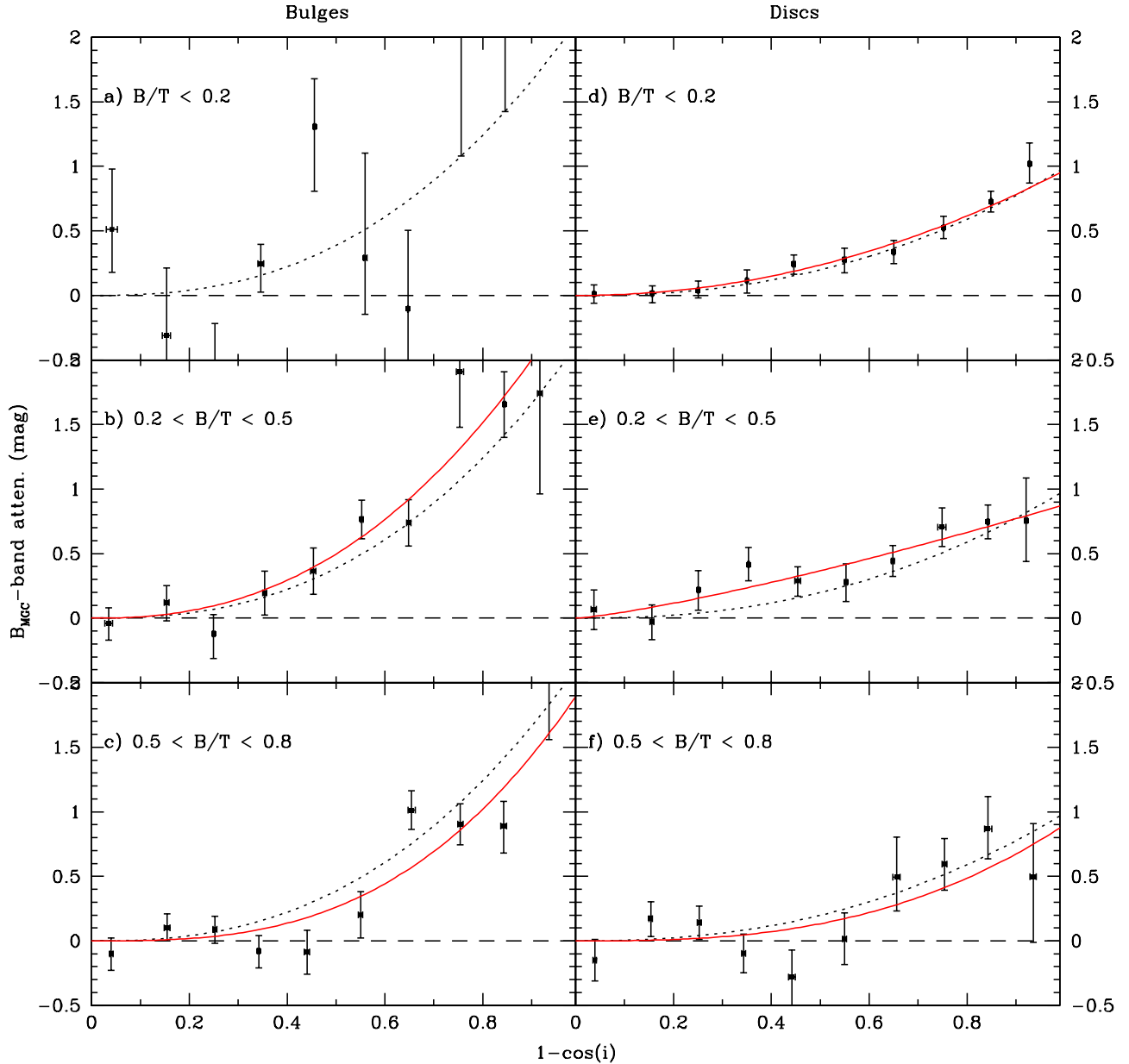


Figure 6. The left and right panels show the bulge and disc attenuation–inclination corrections derived from various B/T -selected sub-samples as indicated. The dotted lines show the solutions derived for the full samples and the solid lines show the final fits for the specified B/T interval.

high signal-to-noise bulge. This is to be expected as the B/T selection ensures that only very high signal to noise discs contribute to the bulge repeats naturally leading to a more accurate inclination measurement. Our conclusion is that our GIM2D results are robust as demonstrated by the repeatability of the measurements. However we cannot rule out certain limitations in the GIM2D software, for example non-exponential discs and disc truncation issues which are not as yet incorporated in the GIM2D package.

3.1.6 Looking at images

A result as strong as that revealed above should be detectable by directly inspecting the imaging data. Fig. 9 shows galaxies with $B/T < 0.2$ drawn from a narrow redshift interval ($0.05 < z < 0.07$). In each $1 - \cos(i)$ bin (vertical axis) we show the eight brightest galaxies, arranged along the horizontal axis by decreasing luminosity. All galaxies are displayed at the same contrast levels, and even though trends will be to some extent masked by cosmic variance it is apparent that there is progressively less flux as one looks down the sequence in inclination. Clearly some objects lie in erroneous positions. For example there is a highly inclined galaxy

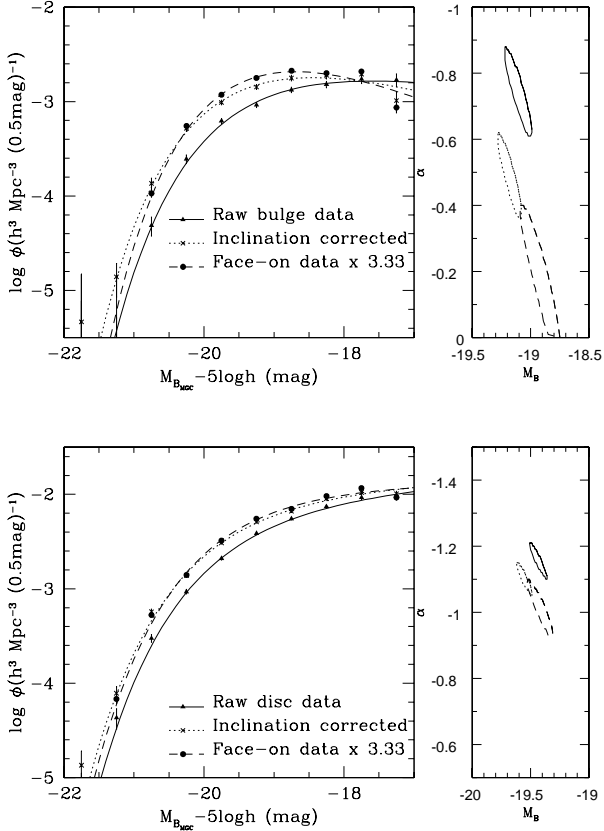


Figure 7. The upper panel shows the bulge luminosity distribution and function before (solid line) and after (dotted line) applying the attenuation–inclination correction. The dashed line shows the luminosity function derived only from face-on [$1 - \cos(i) < 0.3$] data and scaled up by a factor of 3.33. The lower panel shows the same for discs. The right panels show the 1σ error contours in the $M^* - \alpha$ plane.

in the $1 - \cos(i) = 0.4$ to 0.5 bin and highly asymmetric systems are also seen in inappropriate inclination bins. We estimate, roughly, that we have a 10 per cent failure rate in our GIM2D-derived structural catalogue but no systematic bias sufficiently large to dominate our result.

4 MODELLING THE FACE-ON ATTENUATION

In the previous section we obtained a purely empirical attenuation–inclination relation. However, this relation does not provide the face-on attenuation, nor does it give direct information about the dust mass which is needed to account for the observed rise in attenuation with inclination. However, both these quantities can be estimated using a model incorporating a given geometry for the distributions of dust and luminosity, since such models predict both the face-on attenuation and the rise in attenuation with inclination as a function of disc opacity. To derive these we adopt the model of Popescu et al. (2000), which uses geometries for stars and dust which can reproduce the entire UV/optical/FIR/sub-mm spectral energy distribution (SED) of nearby spiral galaxies and for which Tuffs et al. (2004) tabulated the total attenuation versus inclination as a function of central B -band face-on optical depth, τ_B^f , separately for the disc and bulge components.

The predictions of this model for three values of central face-

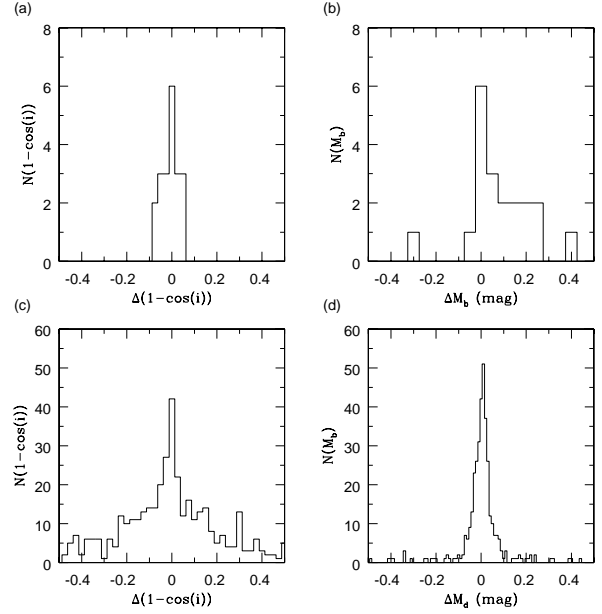


Figure 8. The stability of the key GIM2D measurements of $1 - \cos(i)$ (left panels) and component magnitude (right panels) for bulges (upper panels) and discs (lower panels) for which repeat measurements with GIM2D exist. Note that the adopted inclination for bulge components is taken from their associated discs.

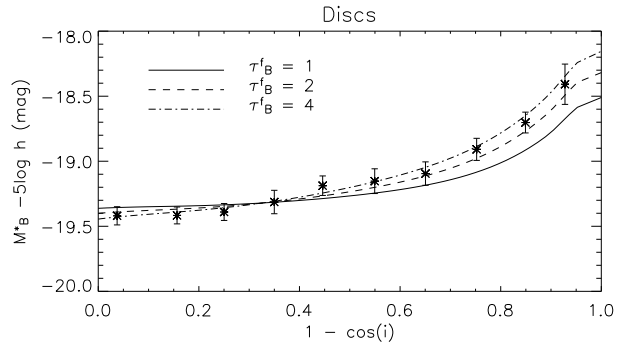


Figure 10. The empirical disc attenuation–inclination relation derived in Section 3 (plotted as symbols) compared to the predictions of the dust model of Tuffs et al. (2004) for discs with different central face-on B_{MGC} -band opacities, τ_B^f .

on B_{MGC} -band opacities $\tau_B^f = 1, 2$ and 4 are overlaid on the $B/T < 0.2$ disc data in Fig. 10. We only consider disc dominated galaxies here in order to minimise any contamination from bulges arising from any biases in the bulge–disc decomposition due to the effect of dust itself. One can see that the model predicts the data rather well for $\tau_B^f = 4$. The best fit is $\tau_B^f = 3.8 \pm 0.7$. From this value we can now derive the B_{MGC} face-on attenuation for discs of (0.20 ± 0.04) mag and for bulges of (0.84 ± 0.10) mag.

This level of attenuation implies that the central regions of disc systems are optically thick, as also found by Shao et al. (2007) based on an analysis of spiral galaxies (without bulge–disc decomposition) drawn from the Sloan Digital Sky Survey (SDSS). To put this in context, consider the case of a geometrically infinitely thin, optically thick disc. In this case one expects all of the light from the far side of the bulge to be entirely blocked. This would result in

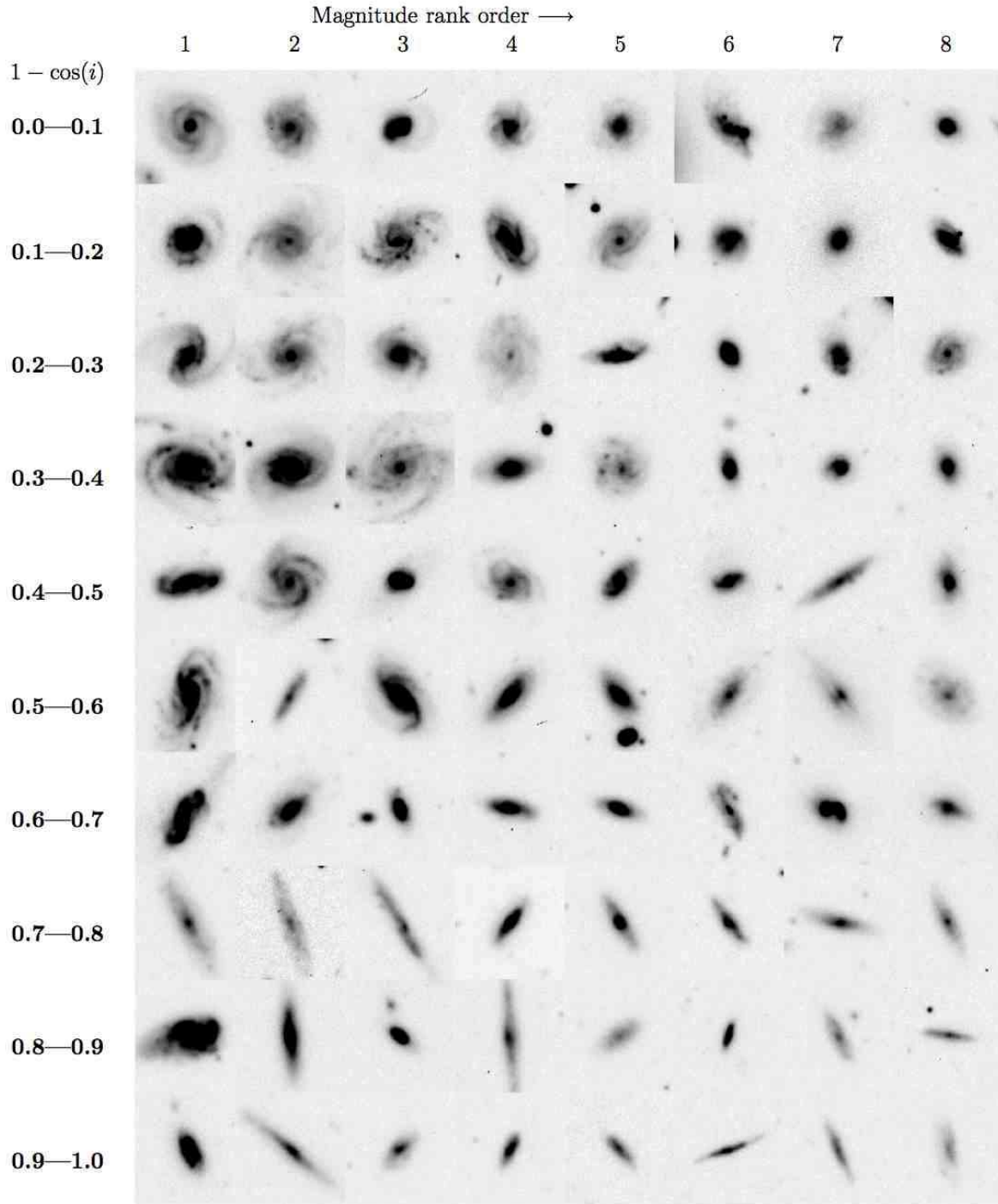


Figure 9. For each $1 - \cos(i)$ bin along the vertical axis we show MGC postage stamp images of the eight brightest galaxies in a narrow redshift interval ($0.05 < z < 0.07$) and with $B/T < 0.2$. Within each bin the galaxies are arranged along the horizontal axis according to their magnitude rank. On average, and in the absence of dust, the galaxies should have the same intrinsic luminosity around the L^* value, irrespective of their inclination. However, one can see a general diminishing of flux towards higher inclination.

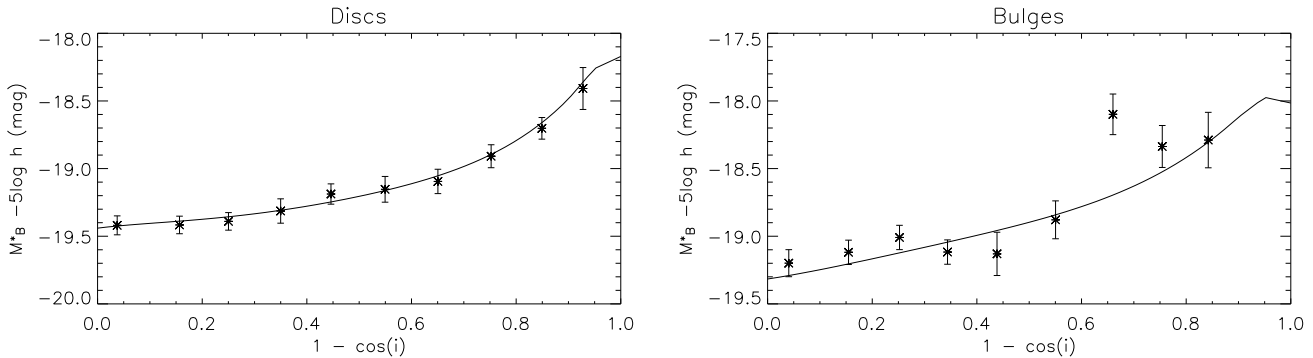


Figure 11. The disc (left) and bulge (right) empirical attenuation–inclination relation derived in Section 3 compared to the prediction of the dust model of Tuffs et al. (2004) with a central face-on B_{MGC} -band opacity $\tau_B^f = 3.8$, as derived from the best fitting solution for the attenuation–inclination relation for discs (see Fig. 10).

a reduction of the bulge’s flux by a factor of two, i.e. by 0.75 mag. We find a slightly higher value of 0.84 mag which reflects the physical thickness of the dust layer. For an infinitely thin disc, one also expects the bulge flux to increase again sharply in the edge-on case where one can see both halves of the bulge. This does not happen in our models, again because of the thickness of the dust layer. Instead, the attenuation decreases only slightly as the edge-on case is approached. The high level of face-on attenuation of bulges derived from our models is quite insensitive to the assumed distribution of unattenuated stellar light in the centre, for example it does not change much when changing the Sérsic index of the bulge. The biggest uncertainty which could potentially affect our conclusion, that more than half of the light from the bulge is blocked by the dust in the disk, concerns whether or not this dust has a hole in the centre. We do not believe this to be the case since imaging observations of dust emission from nearby face-on spiral galaxies (at linear resolutions of a few hundred parsecs or better) show no evidence for an incomplete dust disk in the central regions occupied by the bulge (Haas et al. 1998 and Gordon et al. 2006 for M31; Hippelein et al. 2003 and Hinz et al. 2004 for M33, Popescu et al. 2005 for M101).

Fig. 11 shows the empirically determined attenuation–inclination curve for the bulges of bulge-dominated galaxies, together with the model prediction for $\tau_B^f = 3.8$. The model is broadly consistent with the data. As predicted by Tuffs et al. (2004), the curve is steeper for bulges than for discs, even at low inclinations. It is worth highlighting that the models used here incorporate only one free parameter, τ_B^f , fitted to the discs which provides a satisfactory fit to the full trend for both discs and bulges simultaneously. This suggests that the large scale geometry of dust in the MGC galaxies relative to the stars is well described by that adopted *a priori* by the model. It also follows that the basic model assumption, namely that the effective radius of the bulge is much smaller than the scale-length of the dust disc, is indeed valid for the bulk of galaxies in the sample, irrespective of the value of B/T (cf. the discussion in Section 3.1.3). It also begs the question as to whether entirely embedded bulges may exist in some systems.

We also note that our conclusion that the measured attenuation–inclination curves require galaxies with fairly opaque central regions is qualitatively consistent with the lack of a strong increase in the central surface brightness of the galaxies depicted in Fig. 9 as one progresses from face-on to edge-on sys-

tems. Such an increase is predicted for optically thin galaxies (Möllenhoff et al. 2006).

5 THE COSMIC STELLAR LUMINOSITY, MASS AND DUST DENSITIES

5.1 Intrinsic luminosity functions and the cosmic stellar luminosity density

Having derived the empirical attenuation–inclination relation and the model dependent face-on attenuation for both discs and bulges we are now in a position to derive the luminosity functions of the pre-attenuated B_{MGC} flux produced by the total stellar population (i.e., before any attenuation occurs). To do this we follow Driver et al. (2007) after first applying our attenuation–inclination relation to all discs and bulges derived from systems with post-corrected B/T values ranging up to the relatively large value of 0.8. The validity of also correcting bulge dominated systems is demonstrated by our own data, which show that galaxies with $0.5 < B/T < 0.8$ are attenuated almost as much by dust as galaxies with $0.2 < B/T < 0.5$ (see Figs. 6b and c), and by the local examples of the Centaurus A and Sombrero galaxies. Furthermore, many S0 galaxies obey the FIR–radio correlation, showing that they have similar dust opacities in relation to their star-formation activity as spiral galaxies (Bally & Thronson 1989). Note that it is not clear, at this stage, whether the S0s in our sample are predominantly found among our high- B/T or elliptical populations. Most likely they fall in both. Higher spatial resolution imaging is required before they can be identified with any confidence and hence at this point we cannot make any reliable statements about their dust content.

Fig. 15 and Table 1 show the final results based on both the inclination and the combined inclination and face-on corrections. In making these corrections we assumed that opacity does not depend on luminosity, i.e. we applied the same correction for all galaxies. The recent study by Shao et al. (2007) suggests this assumption is reasonable as they find minimal change in opacity with luminosity.

We note that all three Schechter parameters have been substantially modified by taking into account the effects of dust. This is especially true for bulges, where L^* is increased by a factor of 2.3, ϕ^* is increased by 58 per cent and α is increased by 0.19. This change in α is caused by objects previously below the flux cut-off being dust corrected into the sample. The luminosity densities cor-

responding to the various Schechter function fits are also given in Table 1.

5.2 The cosmic stellar mass densities

In addition to the luminosity densities we also derive the stellar mass densities (Table 1, column 6). We follow the procedure outlined in Driver et al. (2006) which uses the $(g-r)$ disc or bulge colour to derive a mass-to-light ratio based on the prescription given by Bell & de Jong (2001). The adopted equation (see Driver et al. 2006) is:

$$\mathcal{M} = 10^{[1.93(g-r)-0.79]} 10^{-0.4(M_B - M_\odot)}, \quad (4)$$

where \mathcal{M} denotes stellar mass, and $g-r$ and M_B refer to attenuation free quantities. Since we have already corrected the magnitudes for attenuation we must now also correct the colour for the effect of dust before we can apply this formula. Fig. 12 shows the combined correction for attenuation and reddening for an example point on the mass-to- B -band light ratio versus $g-r$ colour relation, separately for discs and bulges. This correction was derived from Tables 4 and 6 of Tuffs et al. (2004) for $\tau_B^f = 3.8$ and for 11 inclinations corresponding to $1 - \cos(i) = 0, 0.1, \dots, 1$. One sees a strong dependence of the corrections on inclination. The colour corrections are listed in Table 2 and are derived from our disc opacity constraint on the general dust models presented in Tuffs et al. (2004). Empirically we cannot determine the absolute colour corrections to corroborate these values, however we can compare the inclination-dependent component. Fig. 13 shows the mean component $(g-r)$ -colour from within each inclination bin. As can be seen from a comparison of the models and data the inclination-dependent colour correction is actually quite weak but in full agreement for discs across the entire inclination range and for bulges with $1 - \cos(i) < 0.6$.

Bell & de Jong argue that the stellar masses derived from their relation are robust against the effect of dust provided the dust vectors are parallel to the relation. The reason is that the under-prediction of stellar mass arising from the attenuation in luminosity will be compensated by the over-prediction of stellar mass arising from the reddening in colour. Inspection of Fig. 12 shows that whereas this balance applies for face-on systems (both for discs and bulges) this is not the case for highly inclined systems. Both bulges and discs at higher inclinations show a systematically higher ratio of attenuation to reddening. This situation arises because a larger fraction of the lines of sight through both bulges and the central regions of discs at all inclinations are optically thick, and in the optically thick limit attenuation becomes saturated at a high level, exhibiting only a small variation with wavelength (see Tuffs et al. 2004). The overall consequence is that stellar masses will be under-predicted for a randomly oriented distribution by use of the Bell & de Jong relation if dust is not taken into account.

The corrections shown in Fig. 12 were applied to each object individually and the stellar masses were extracted using equation (4). These estimates for the mass densities (as well as for the stellar luminosity) will be valid if the efficiency of absorption of B_{MGC} -band photons by M^* galaxies is representative of the galaxy population at large.

In order to ascertain the credibility of our stellar mass estimates we compare our masses to those derived for SDSS galaxies by Kauffmann et al. (2003). The data were kindly provided by J. Brinchman (priv. comm.) and were matched to the MGC catalogue, resulting in 1855 matched objects (using a 5 arcsec positional tolerance). The relatively small number of matches is

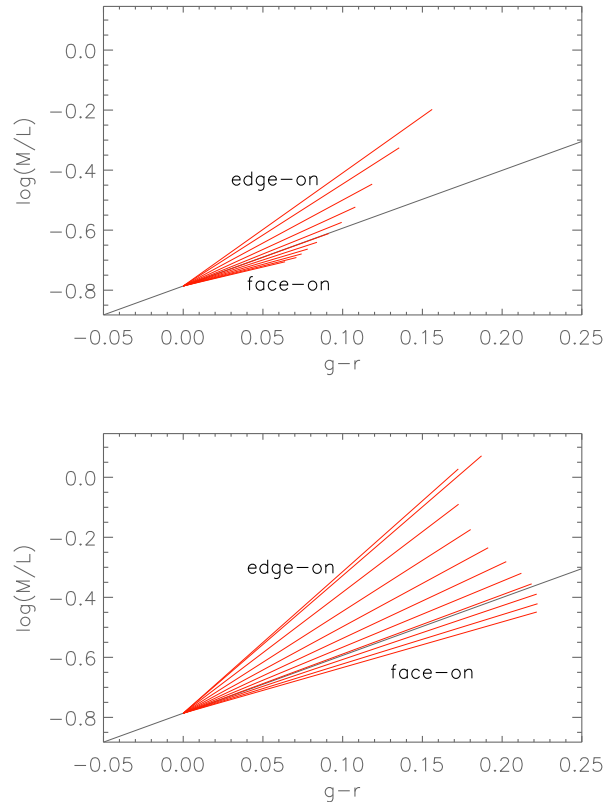


Figure 12. This figure shows the predicted relation (black line) between intrinsic mass-to- B -band light ratio and intrinsic $g-r$ colour, derived by Bell & de Jong (2001) for a fixed total stellar mass. We over-plot 11 vectors in red showing the shift of a point on the correlation due to dust for inclinations $1 - \cos(i) = 0, 0.1, \dots, 1$. The upper and lower panels show the disc and bulge cases, respectively. The vectors are calculated from the model of Tuffs et al. (2004) for $\tau_B^f = 3.8$. Vectors which move away from the fixed mass locus imply a significant change in the galaxy’s total stellar mass, which appears to be the case for edge on systems.

due to the much brighter limit of the SDSS spectroscopic survey compared to the MGC. The SDSS stellar mass-to-light ratios are derived from the spectra, a dust attenuation correction from the colours and the final masses from the z -band Petrosian fluxes (incorporating the derived mass-to-light ratio and attenuation correction). Full details of this process are given by Kauffmann et al. (2003).

Fig. 14 shows the comparison of the matched sample both with and without dust correction (which applies to both the SDSS and MGC data). Note that we are comparing total-galaxy stellar masses here, i.e. for two-component galaxies we have summed the MGC disc and bulge estimates. The median stellar mass ratio is found to be 1.18 (i.e., 0.073 dex) with SDSS masses being systematically higher. SDSS masses are based on a Kroupa (2001) IMF whereas the Bell & de Jong values are based on a Salpeter-lite IMF but these should give comparable masses. The dispersion is reasonable, implying an uncertainty of $\Delta \log(\mathcal{M}) = \pm 0.16$ (45 per cent) for individual galaxy measurements which includes a contribution from the magnitude uncertainty. If one assumes the stellar mass error is equally distributed between the two surveys this implies individual mass uncertainties of: $\Delta \log(\mathcal{M}) \sim \pm 0.11$ (i.e., 30 per cent). We therefore conclude that our mass estimates show a

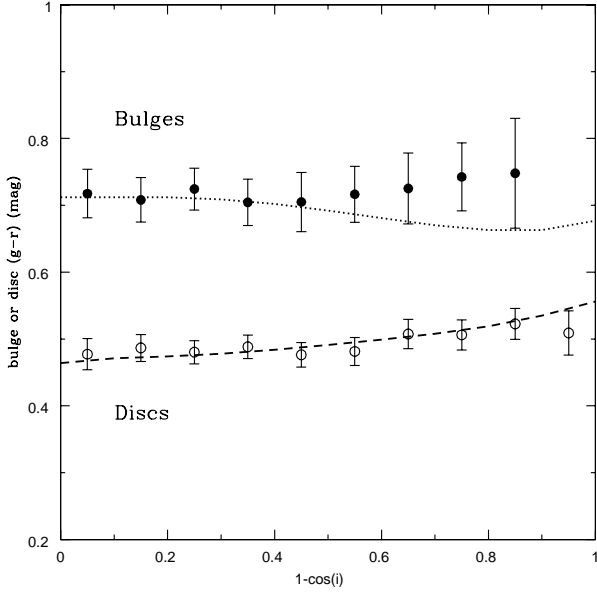


Figure 13. The component- $(g-r)$ colour versus inclination for bulges and discs derived empirically (data points) and predicted by our dust models (lines).

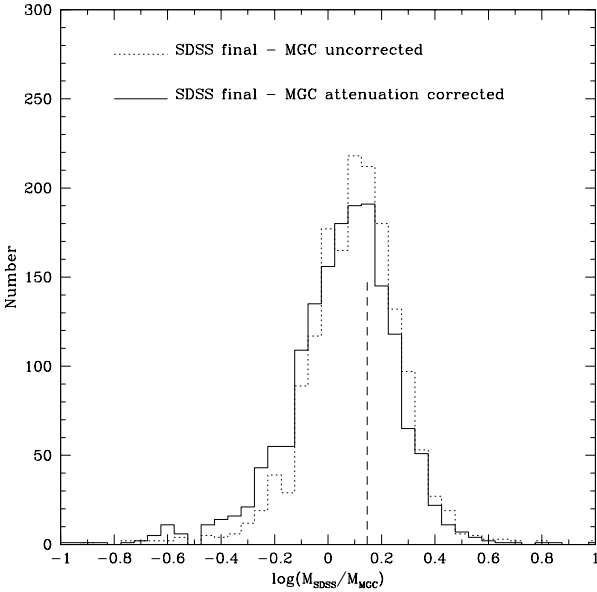


Figure 14. Comparison of the final dust corrected SDSS stellar masses (Kauffmann et al. 2003) and the MGC total-galaxy stellar masses for MGC data with (dotted line) and without (solid line) our dust correction. The corrected MGC data is shifted to higher masses, relative to SDSS values and the final median offset is a factor of ~ 1.18 (i.e., 0.073 dex).

reasonable dispersion but are still systematically lower than SDSS estimates by ~ 18 per cent. Examining the data more closely one can see a trend for more discrepant masses amongst bluer star forming galaxies, this will be explored further in a future paper.

The stellar mass densities shown in column 6 of Table 1 are derived from a simple sum over all bulges or discs, where

Table 2. Inclination dependent $(g-r)$ colour corrections for bulges and discs.

$1 - \cos(i)$	bulge $(g-r)$ corr.	disc $(g-r)$ corr.
0.0	0.222	0.064
0.1	0.222	0.071
0.2	0.222	0.074
0.3	0.219	0.078
0.4	0.212	0.084
0.5	0.202	0.091
0.6	0.191	0.099
0.7	0.180	0.108
0.8	0.173	0.119
0.9	0.173	0.135
1.0	0.187	0.156

each component’s stellar mass is first multiplied by a weight. This weight is the space density at the component’s luminosity (from the relevant luminosity function) divided by the number of systems which contributed to that luminosity interval (see Driver et al. 2006). The values for all parameters (Schechter function, luminosity density and stellar mass density) shown in Table 1 are revised from those shown in Driver et al. (2007), because of the dust correction. It is instructive to compare the final luminosity and stellar mass densities derived from the attenuation–inclination correction and from the rescaled face-on values. In almost all cases we see that the rescaled values are slightly higher; this *may* be a further reflection of residual incompleteness in the highest inclination bin (cf. the $1 - \cos(i)$ distributions of Fig. 5 and the luminosity functions shown in Fig. 7). One can estimate a correction factor to apply to the attenuation corrected data based on the incompleteness of extreme inclination objects. These are 1.05 for bulges and 1.06 for discs resulting in final stellar mass density estimates, at redshift zero, of:

$$\begin{aligned}
 \rho(\text{discs}) &= (4.4 \pm 0.3) \times 10^8 h M_{\odot} \text{Mpc}^{-3} \\
 \rho(\text{bulges}) &= (2.2 \pm 0.2) \times 10^8 h M_{\odot} \text{Mpc}^{-3} \\
 \rho(\text{ellipticals}) &= (0.8 \pm 0.1) \times 10^8 h M_{\odot} \text{Mpc}^{-3}
 \end{aligned} \tag{5}$$

Hence we conclude that the combined stellar mass density based on our empirical inclination plus model face-on correction is $\rho = (7.6 \pm 0.4 \pm 1.0) \times 10^8 h M_{\odot} \text{Mpc}^{-3}$, where the second error is due to cosmic variance. This should be modified downwards by about a factor of 1.1 to get a Kroupa IMF based value (I. Baldry priv. comm.). Note that this total value also includes the stellar mass estimate, derived in Driver et al. (2007), for the low luminosity blue spheroid systems of $\rho(\text{blue spheroids}) = (0.2 \pm 0.1) \times 10^8 h M_{\odot} \text{Mpc}^{-3}$.

5.3 The cosmic dust density

The derivation of the cosmic dust density from the MGC data is less straightforward, as there is no obvious direct physical link between the mass of dust in a galaxy and the B -band luminosity. Neither is there direct empirical information linking these two quantities over the luminosity range covered by the MGC due to the lack of statistically significant FIR or sub-mm measurements of galaxies less luminous than M^* . Here we simply assume that there is a fixed ratio between dust mass and B_{MGC} -band intrinsic luminosity of discs, as adopted for the canonical galaxy model used by Tuffs

Table 1. Schechter function parameters for various galaxy samples with varying degrees of dust attenuation corrections.

Component	$M^* - 5 \log h$ (mag)	ϕ^* ($10^{-2} h^3 \text{ Mpc}^{-3} (0.5 \text{ mag})^{-1}$)	α	j^a ($10^8 h L_\odot \text{ Mpc}^{-3}$)	ρ^b ($10^8 h M_\odot \text{ Mpc}^{-3}$)
Discs:					
uncorrected	-19.45 ± 0.04	1.8 ± 0.1^d	-1.16 ± 0.04	1.7 ± 0.2^d	3.8 ± 0.4^d
inclination corrected	-19.56 ± 0.04	$2.1(2.2)^c \pm 0.1^d$	-1.10 ± 0.03	$2.1(2.2)^c \pm 0.2^d$	$4.7(5.0)^c \pm 0.5^d$
inclination & face-on corrected	-19.76 ± 0.04	$2.1(2.2)^c \pm 0.1^d$	-1.11 ± 0.03	$2.6(2.7)^c \pm 0.2^d$	$4.1(4.4)^c \pm 0.3^d$
$3.33 \times (1 - \cos(i) < 0.3)$	-19.44 ± 0.07	2.7 ± 0.2^d	-1.02 ± 0.06	2.3 ± 0.5^d	5.3 ± 1.2^d
$3.33 \times (1 - \cos(i) < 0.3)$ & face-on corrected	-19.64 ± 0.07	2.6 ± 0.2^d	-1.04 ± 0.05	2.7 ± 0.5^d	4.7 ± 0.9^d
Bulges:					
uncorrected	-19.11 ± 0.07	0.65 ± 0.05^d	-0.75 ± 0.08	0.37 ± 0.06^d	1.6 ± 0.3^d
inclination corrected	-19.18 ± 0.07	$0.87(0.91)^c \pm 0.05^d$	-0.49 ± 0.08	$0.51(0.54)^c \pm 0.06^d$	$2.3(2.4)^c \pm 0.3^d$
inclination & face-on corrected	-20.00 ± 0.07	$0.97(1.03)^c \pm 0.05^d$	-0.56 ± 0.08	$1.22(1.29)^c \pm 0.15^d$	$2.1(2.2)^c \pm 0.2^d$
$1 - \cos(i) < 0.3$	-18.92 ± 0.11	1.23 ± 0.07^d	-0.19 ± 0.15	0.60 ± 0.08^d	2.7 ± 0.4^d
$1 - \cos(i) < 0.3$ & face-on corrected	-19.68 ± 0.10	1.27 ± 0.07^d	-0.19 ± 0.15	1.25 ± 0.15^d	2.1 ± 0.3^d
Spheroids (bulges + ellipticals)^e:					
uncorrected	-19.15 ± 0.06	0.99 ± 0.05^d	-0.66 ± 0.07	0.57 ± 0.07^d	2.4 ± 0.4^d
inclination corrected	-19.15 ± 0.06	1.23 ± 0.05^d	-0.44 ± 0.07	0.71 ± 0.08^d	$3.1(3.2)^c \pm 0.4^d$
inclination & face-on corrected	-19.95 ± 0.06	1.37 ± 0.07^d	-0.76 ± 0.05	1.7 ± 0.2^d	$2.9(3.0)^c \pm 0.3^d$
$3.33 \times (1 - \cos(i) < 0.3)$	-19.00 ± 0.05	1.53 ± 0.15^d	-0.31 ± 0.07	0.8 ± 0.1^d	3.5 ± 0.5^d
$3.33 \times (1 - \cos(i) < 0.3)$ & face-on corrected	-19.75 ± 0.04	1.61 ± 0.15^d	-0.52 ± 0.05	1.6 ± 0.2^d	2.9 ± 0.4^d
Ellipticals (no corrections)	-19.02 ± 0.11	0.37 ± 0.03^d	-0.26 ± 0.14	0.20 ± 0.03^d	0.8 ± 0.1^d

^aThe luminosity density is defined as $j = \phi^* L^* \Gamma(\alpha + 2)$, where we use $M_\odot = 5.38 \text{ mag}$. To convert from the B_{MGC} to the b_J -band multiply all j values by 1.05.

^bThe stellar mass density is derived using equation (4). The colour corrections shown in Table 2 are only used when calculating face-on corrected values.

^cAll ϕ^* , j and ρ values for inclination corrected data and inclination and face-on corrected data can arguably be scaled up by factors of 1.05 for bulges and 1.06 for discs if one wishes to compensate for the apparent incompleteness in the highest inclination bin of Fig. 5.

^dThe quoted errors on ϕ^* , j and ρ are the random errors only. Based on mock 2dFGRS NGP catalogues (Cole et al. 1998) we estimate that the potential systematic error on these values due to cosmic variance amounts to 13 per cent.

^eAll corrections and the $\cos(i)$ selection are only applied to the bulges. No corrections are applied to the ellipticals.

et al. (2004) for M^* , and scale the cosmic B_{MGC} -band luminosity density of discs, as derived in Section 5.1, by this ratio.

As it is mainly discs close to M^* which dominate the total disc luminosity density, a luminosity dependent dust mass-to-light ratio would not actually be problematic as long as the dependency is not extreme. In this context we note that our value for the opacity of discs ($\tau_B^f = 3.8 \pm 0.7$) is comparable to that obtained from detailed SED modelling of the components of stellar luminosity absorbed by grains and re-radiated in the FIR (Popescu et al. 2000; Misiriotis et al. 2001; Misiriotis et al. 2004) of well studied, relatively luminous L^* spiral galaxies. We augment this sample with data for spiral and dwarf galaxies with *ISO* detections drawn from Tuffs et al. (2002), for which Popescu et al. (2002) derive dust masses for 29 galaxies with FIR and B -band luminosity measurements. In these systems, the ratio of dust mass per B -band disc intrinsic luminosity is found to be $(0.00196 \pm 0.00058) M_\odot L_\odot^{-1}$ (note no h dependence). Multiplying this ratio by the intrinsic B_{MGC} luminosity density of discs of $2.7 \times 10^8 h L_\odot \text{ Mpc}^{-3}$ then yields a value of $(5.3 \pm 1.6 \pm 0.7) \times 10^5 h M_\odot \text{ Mpc}^{-3}$ for the cosmic dust density, where the second error is due to cosmic variance.

5.4 Implications for the cosmic baryon budget

Adopting a value for the total cosmic baryon density of $\Omega_{\text{baryon}} h^2 = 0.023$ (Tegmark et al. 2006) and $\rho_{\text{crit}} = 2.7755 \times 10^{11} h^2 M_\odot \text{ Mpc}^{-3}$, we find the fraction of cosmic baryons in dust and stars today is $(0.0083 \pm 0.0027) h$ per cent and $(11.9 \pm 1.7) h$ per cent (Salpeter-lite), respectively. This value for the stel-

lar baryon fraction is marginally (2σ) higher than that previously derived by Baldry & Glazebrook (2003) of $(5 - 9) h$ per cent (marginalized over a variety of IMFs). Our value is also slightly higher than the value of $(9 \pm 1.3) h$ per cent derived by Cole et al. (2001) from the 2MASS/2dFGRS NIR luminosity function (see also the summary of stellar masses in Bell et al. 2003). We note that Cole et al. (2002) cite their values as dust free but acknowledge that if dust attenuation is severe this could impact upon their estimates. Using our model we can explore this by deriving dust attenuation values for the bulge and disc components in the K_s -band (see Fig. 16) which demonstrate that dust attenuation remains non-negligible even at K_s .

6 SUMMARY AND DISCUSSION

We have demonstrated that dust attenuation is a severe issue in the B -band, resulting in the magnitudes of both discs and bulge components being severely underestimated by factors of 0.20–1.1 mag and 0.84–2.6 mag respectively. The direct implication is that only 63 and 29 per cent of the total B -band photons produced by stars in discs and bulges, respectively, actually make it out of the galaxy (as deduced from the luminosity densities with and without dust corrections). The remainder are absorbed by the dust and presumably re-radiated in the FIR. As this re-radiation is likely to be almost perfectly isotropic and un-attenuated one might expect the optical to FIR flux ratio to show some inclination dependence. We find that the central face-on optical depth of discs is $\tau_B^f = 3.8 \pm 0.7$ which implies that discs are optically thick in the centres. This conclusion

was also reached by Shao et al. (2007) who analysed the behaviour of total-galaxy magnitudes of spiral galaxies drawn from the SDSS as a function of inclination. We find that this conclusion holds regardless of the bulge luminosity and it is hence independent of the bulge-to-total flux ratio. Thus, dust appears to be inherently related to the disc, with no physical connection to the bulges.

Our value for the opacity of discs ($\tau_B^f = 3.8 \pm 0.7$) is comparable to that obtained from self-consistent SED modelling of the components of stellar luminosity absorbed by grains and re-radiated in the FIR (Popescu et al. 2000, Misiriotis et al. 2001, Misiriotis et al. 2004). This value for central face-on opacity is however significantly higher than might be expected on the basis of the extinction measurements towards central stellar clusters in spiral galaxies by Sarzi et al. (2005). As a possible explanation for this discrepancy, we note that our measurement of τ_B^f (like that from the SED modelling) is derived from the integrated properties of galaxies. It is therefore representative of the global distribution of opacity over the whole disc, and is not sensitive to opacity along individual lines of sight; in other words, it is not sensitive to inhomogeneities in the dust distribution on scales of 100 pc. Therefore, this difference may indicate that the dust density in the central 100 pc of spiral galaxies may be systematically lower than for the surrounding regions of the inner disc, and that the central 100 pc region may have some specific properties, e.g. due to feedback in the form of dispersion of material surrounding a central massive star cluster. Alternatively, it may simply be that the disc population has a large range of opacities, and that central star clusters are only clearly identifiable in discs with relatively low opacities.

Although this work quantifies the severity of the mean dust attenuation in galaxy discs and bulges this method cannot constrain the galaxy-to-galaxy variation. To address this it is imperative that pointed FIR observations of large, optically selected galaxy samples are undertaken with sufficient depth to detect systems over the full luminosity range sampled by surveys such as the MGC.

In terms of the total B -band luminosity density of the Universe, based on luminosity function estimates, we infer that our previous estimates (Liske et al. 2003, 2006; Driver et al. 2005, 2006, 2007) should be revised upwards by a factor of ~ 1.8 . In terms of the stellar mass density the change amounts to an upward revision of a factor of ~ 1.2 . Previous estimates of the B -band galaxy luminosity function which have neglected to correct for dust attenuation, have underestimated M_B^* by $\sim 0.6 - 1$ mag. When comparing models of galaxy formation and evolution to data one must therefore be careful to either include realistic dust attenuation in the models or to compare to dust corrected data as provided here.

In Driver et al. (2007) we reported that the stellar mass was broken down as 60:27:13 into discs:classical bulges:ellipticals (ignoring the contribution from pseudo-bulges and blue ellipticals). We can now revise these values, incorporating our dust corrections for discs and bulges, to 59:30:11. Hence the stellar mass in classical bulges is a factor of 2.7 higher than the mass in ellipticals.

Throughout this study we have assumed ellipticals to be dust free. Since ellipticals and bulges are known to have similar apparent colours, the correction of our bulges for dust attenuation implies that they will have significantly bluer intrinsic colours. It therefore follows that they must be younger and/or metal poorer which is consistent with the spectroscopic studies of Proctor & Sansom (2002) and Thomas & Davies (2006).

We also note that the high opacities leading to our conclusion that the bulges have intrinsically bluer colours is not inconsistent with the observations that bulges show a small spread in apparent colours and exhibit small colour gradients (see review by Renzini

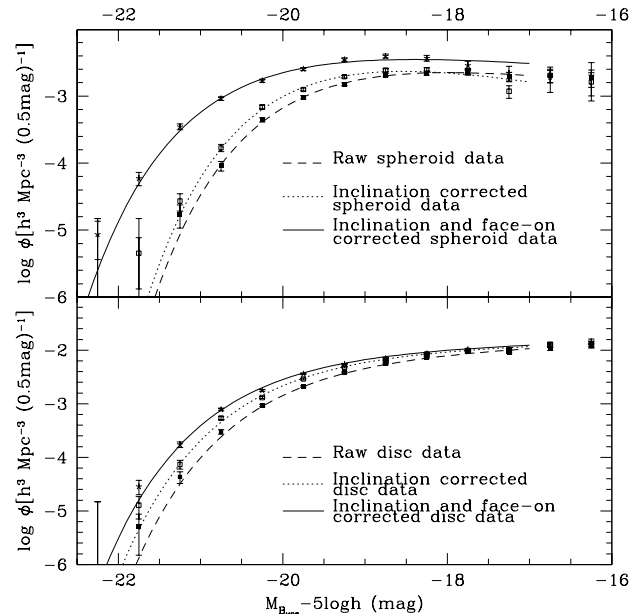


Figure 15. The upper panel shows the spheroid (i.e. bulge+elliptical) luminosity function before and after corrections and the lower panel shows the disc luminosity function before and after corrections.

2006). Our dust model predicts that for the high opacities found in this paper the variation in bulge colour due to dust is almost independent of inclination (see also Section 5.2), and that there should be very little colour gradients in bulges due to dust.

Finally, our calibrated dust model predicts that dust will significantly attenuate stellar light even at NIR wavelengths, particularly for bulges. This is illustrated in Fig. 16 where predicted attenuation–inclination curves are plotted for the bulge and disc components of a $\tau_B^f = 3.8 \pm 0.7$ galaxy in the B , I and K_s bands. Hence even the upcoming deep NIR surveys will need to manage internal dust attenuation with care.

ACKNOWLEDGMENTS

We thank Jarle Brinchman for providing SDSS stellar mass data and Ivan Baldry for comments on earlier drafts. We would also like to acknowledge enlightening discussions with Barry Madore, Alan Dressler and Anne Sansom. The Millennium Galaxy Catalogue consists of imaging data from the Isaac Newton Telescope and spectroscopic data from the Anglo Australian Telescope, the ANU 2.3m, the ESO New Technology Telescope, the Telescopio Nazionale Galileo and the Gemini North Telescope. The survey has been supported through grants from the Particle Physics and Astronomy Research Council (UK) and the Australian Research Council (AUS). The data and data products are publicly available from <http://www.eso.org/~jliske/mgc/> or on request from J. Liske or S.P. Driver.

REFERENCES

- Allen P., Driver S.P., Graham A.W., Cameron E., Liske J., Cross N.J.G., De Propris R., 2006, MNRAS, 371, 2
- Baes M., Dejonghe H., 2001, MNRAS, 326, 733

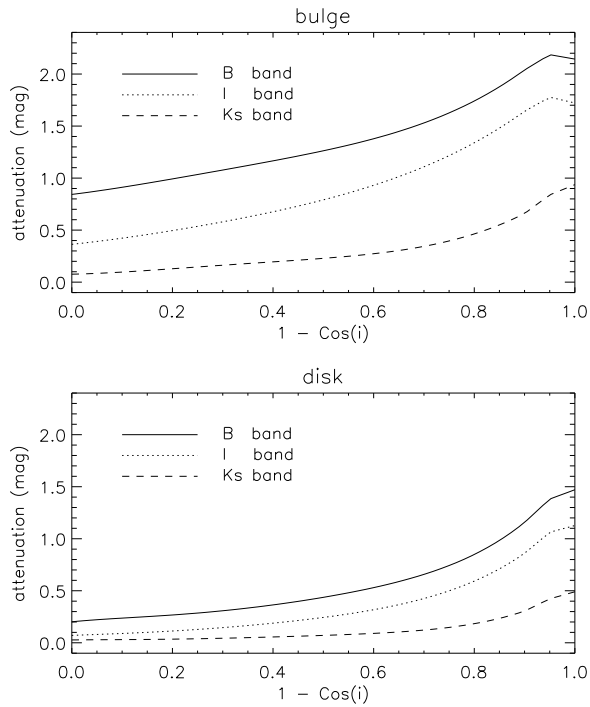


Figure 16. Predicted attenuation–inclination curves in the B , I and K_s bands for the bulge (top panel) and the disc (lower panel) of a galaxy with a central face-on optical depth in the B_{MGC} -band of $\tau_B^f = 3.8$.

Baldry I., Glazebrook K., 2003, *ApJ*, 593, 258
 Bally J., Thronson H.A. Jr, 1989, *AJ*, 97, 69
 Bell E.F., de Jong, R.S., 2001, *ApJ*, 550, 212
 Bell E.F., McIntosh D.H., Katz N., Weinberg M.D., 2003, *ApJS*, 149, 289
 Bianchi S., Ferrara A., Giovanardi C., 1996, *ApJ*, 465, 127
 Bianchi S., Davies J.I., Alton P.B., 2000, *A&A*, 359, 65
 Blanton M. et al., 2003, *ApJ*, 592, 819
 Boissier S., Boselli A., Buat V., Donas J., Milliard B., 2004, *A&A*, 424, 465
 Byun Y.I., Freeman K.C., Kylafis N.D., 1994, *ApJ*, 432, 114
 Choi Y., Park C., Vogeley M.S., 2006, *ApJ*, in press, astro-ph/0611607
 Cole S., Hatton S., Weinberg D.H., Frenk C.S., 1998, *MNRAS*, 300, 945
 Cole S. et al., 2001, *MNRAS*, 326, 255
 Cross N.J.G., Driver S.P., Liske J., Lemon D.J., Peacock J.A., Cole S., Norberg P., Sutherland W.J., 2004, *MNRAS*, 349, 576
 Cunow B., 2001, *MNRAS*, 323, 130
 Davies J.I., Burstein D., 1995, in *The opacity of spiral discs*, NATA ASI, (Publ: Kluwer)
 Disney M.J., Davies J.I., Phillipps S., 1989, *MNRAS*, 239, 939
 Disney M.J., Burstein D., Haynes M.P., Faber S.M., 1992, *Nature*, 356, 114
 Driver S.P., Liske J., Cross N.J.G., De Propris R., Allen P.D., 2005, *MNRAS*, 360, 81
 Driver S.P. et al., 2006, *MNRAS*, 368, 414
 Driver S.P., Allen P., Liske J., Graham A.W., 2007, *ApJL*, submitted
 Efstathiou G., Ellis R.S., Peterson B.A., 1988, *MNRAS*, 232, 431
 Evans R., 1994, *MNRAS*, 266, 511
 Ferrara A., Bianchi S., Cimatti A., Giovanardi C., 1999, *ApJS*,

123, 437
 Giovanelli R., Haynes M.P., Salzer J.J., Wegner G., da Costa L.N., Freudling W., 1995, *AJ*, 110, 1059
 Gordon K.D., et al. 2006, *ApJ*, 638, 87
 Graham A.W., 2001, *MNRAS*, 326, 543
 Graham A.W., Driver S.P., 2004, *PASA*, 22, 118
 Graham A.W., Driver S.P., Petrosian V., Conselice C., Bershadsky M., Crawford S.M., Tomotsugu G., 2005, *AJ*, 130, 1535
 Hass M., Lemke D., Stickel M., Hippelein H., Kunkel M., Herbstmeier U., Mattila K., 1998, *A&A*, 338, 33
 Hinz J.L., et al., 2004, *ApJS*, 154, 259
 Hippelein H., Haas M., Tuffs R.J., Lemke D., Stickel M., Klaas U., Volk, H.J., 2003 *A&A*, 407, 137
 Holmberg E., 1946, *Medd. Lunds Obs. II*, No. 117
 Holmberg E., 1958, *Medd. Lunds Obs. II*, No. 136
 Hubble E., 1926, *ApJ*, 64, 321
 Kauffmann G. et al., 2003, *MNRAS*, 341, 33
 Keel W.C., White R.E. III, 2001, *AJ*, 122, 1369
 Kuchinski L.E., Terndrup D.M., Gordon K.D., Witt A.N., 1998, *AJ*, 115, 1438
 Kylafis N.D., Bahcall J.N., 1987, *ApJ* 317, 637
 Liske J., Lemon D., Driver S.P., Cross N.J.G., Couch W.J., 2003, *MNRAS*, 344, 307
 Liske J., Driver S.P., Allen P.D., Cross N.J.G., De Propris R., 2006, *MNRAS*, 369, 1547
 Masters K.L., Giovanelli R., Haynes M.P., *AJ*, 126, 158
 Misiriotis A., Popescu C.C., Tuffs R.J., Kylafis N.D., 2001, *A&A*, 372, 775
 Misiriotis A., Papadakis I.E., Kylafis N.D., Papamastorakis J., 2004, *A&A*, 417, 39
 Möllenhoff C., Popescu C.C., Tuffs R.J., 2006, *A&A* 456, 941
 Norberg P. et al., 2001, *MNRAS*, 336, 907
 Östman L., Goobar A., Mortzell E., 2006, *A&A*, 450, 971
 Pierini D., Maraston C., Gordon K.D., Witt A.N., 2005, *MNRAS*, 363, 131
 Poggianti B., 1997, *A&AS*, 122, 399
 Popescu C.C., Misiriotis A., Kylafis N.D., Tuffs R.J., Fischera J., 2000, *A&A*, 362, 138
 Popescu C.C., Tuffs R.J., Völk H.J., Pierini D., Madore B.F., 2002, *ApJ*, 567, 221
 Popescu C.C., Tuffs R.J., 2005, in "The Spectral Energy Distribution of Gas-Rich Galaxies: Confronting Models with Data", Heidelberg, 4-8 Oct. 2004, eds. C.C. Popescu & R.J. Tuffs, AIP Conf. Ser., 761, 155
 Popescu C.C. et al., 2005, *ApJL*, 619, L75
 Proctor R.N., Sansom A.E., 2002, *MNRAS*, 333, 517
 Renzini A., 2006, *ARAA*, 44, 141
 Sarzi M., Rix H.-W., Shields J.C., Ho L.C., Barth A.J., Rudnick G., Filippenko A.V., Sargent W.L.W., 2005, *ApJ*, 628, 169
 Shao Z., Xiao W., Shen S., Mo H.J., Xia X., Deng Z., 2006, *ApJ*, in press, astro-ph/0611714
 Shen S. et al., 2003, *MNRAS*, 343, 978
 Silva L., Granato G.L., Bressan A., Danese L., 1998, *A&A*, 509, 103
 Simard L. et al., 2002, *ApJS*, 142, 1
 Tegmark M. et al., 2006, *Phys. Rev. D*, 74, 123507
 Thomas D., Davies R.L., 2006, *MNRAS*, 366, 510
 Tuffs R.J. et al., 2002, *ApJS*, 139, 37
 Tuffs R.J., Popescu C.C., Völk H.J., Kylafis N.D., Dopita M.A., 2004, *A&A*, 419, 835
 Valentijn E.A., 1990, *Nature*, 346, 153

Xilouris E.M., Byun Y.I., Kylafis N.D., Paleologou E.V., Papatourakis J., 1999, *A&A*, 344, 868
Zucca E. et al., 1997, *A&A*, 326, 477